Heliyon 5 (2019) e02729

Contents lists available at ScienceDirect

Heliyon

journal homepage: www.heliyon.com

Research article

NIR light active ternary modified ZnO nanocomposites for combined cancer therapy

K. Vasuki, R. Manimekalai *

Department of Chemistry, Kongunadu Arts and Science College, Coimbatore, 641 029, Tamilnadu, India

ARTICLE INFO

Keywords:
Inorganic chemistry
Materials chemistry
Pharmaceutical chemistry
Nanocomposites
Zinc oxide
NIR
In vitro cytotoxicity
PTT
PDT

ABSTRACT

Recent developments in nanomedicine for cancer therapy enable nanoparticles for tumour specific therapeutics. Certain nanoparticles with their inherent physical/chemical properties can themselves act as drugs. Also they can be designed to respond to either tumor microenvironment or externally applied physical stimuli such as temperature, light, magnetic field, and ultrasound for tumor-targeted and enhanced anticancer efficacy. In this study, a simple design of cost-effective ternary modified zinc oxide nanocomposites possessing near-infrared (NIR) absorbance were synthesized using simple, fast, thermal decomposition route with hydrazine precursors. The in vitro cytotoxicity of these nanocomposites studied on human breast cancer cells (MCF-7) and the human embryonic kidney normal cells (HEK 293) by MTT assay show that they are highly selective and are dose dependent against both the cell lines. The developed nanocomposites can be used for combined photothermal (PTT) and photo dynamic (PDT) cancer therapy.

1. Introduction

Today cancer is one of the leading causes of death worldwide, which is mainly treated with chemo therapy, radiation, and surgery. While chemotherapy and radiotherapy suffer from severe toxic side effects to normal tissues, surgery in most occasions could not remove all cancer cells in the human body. Nanotechnology and nanomedicine can offer a more targeted approach in the treatment of cancer. Nanoparticles with their small size preferentially enter into the leaky vascular tumour tissues, and are then retained in the tumour bed, by a process recognized as the enhanced permeation and retention (EPR) effect [1]. In this regard, metal oxide semiconductor nanoparticles is of interest, as they can participate in cellular redox reactions and have photocatalytic activity [2]. Zinc oxide (ZnO) belonging to a group of metal oxides is a wide band-gap semiconductor which absorbs in the UV region. ZnO NPs are biocompatible having antibacterial properties and show inherent differential toxicity against rapidly dividing cancer cells [3, 4, 5]. Generation of intracellular reactive oxygen species (ROS) is a major cytotoxic mechanism of ZnO NPs leading to cell death [6, 7]. For nanoscale ZnO large numbers of valence band holes and/or conduction band electrons are available on the surface due to crystal defects. These electron-hole pairs get trapped by dissolved oxygen in the aqueous solution inside the cell resulting in the production reactive of oxygen species (ROS). Generally cancer cells themselves produce more ROS than normal cells owing to their faster metabolic rate. Therefore, exogenous ROS-generating agents like ZnO NPs produces more ROS in cancer cells than normal cells resulting in huge oxidative stress in the cancer cell and eventually killing the cell [8, 9]. The selective toxicity of ZnO NPs can further be improved by external stimulation like photo activation.

Phototherapeutics, involving photodynamic therapy (PDT) and photothermal therapy (PTT) using nanomaterials have received attention, due to their selective and localized therapeutic effect by light irradiation [10]. PDT, a minimally invasive method for treating cancer, uses photosensitizing agents which upon exposure to cancer cells can produce toxic reactive oxygen species (ROS) such as hydroxyl radical, hydrogen peroxide, and superoxide under light irradiation leading to cancer cell death [11]. PTT is also a minimally invasive therapeutic strategy, where light irradiation is converted by photothermal agents to heat, leading to thermal ablation of cancer cells with subsequent death of the malignant cells [12]. The photothermal agents for PTT should have absorption in the near infrared region (NIR) (700–2500 nm) which is a transparency window for biological tissues. Dual-modal phototherapeutics that combine PDT and PTT can have synergistic effects which enhance the therapeutic efficacy compared to PDT or PTT alone [13, 14]. Photoabsorbing agents with improved efficiency of reactive oxygen species (ROS) generation, high absorption, photostability and near-infrared

* Corresponding author.
E-mail address: rmanimekalai12@gmail.com (R. Manimekalai).

https://doi.org/10.1016/j.heliyon.2019.e02729
Received 21 August 2019; Received in revised form 30 September 2019; Accepted 22 October 2019

(NIR) light absorption are necessary for dual-modal phototherapeutics to treat diseases. Metal based nanoscale materials exhibit higher absorption and have high photostability [15].

Upon UV irradiation ZnO nanoparticles produces more electrons and holes which increases their ability to generate ROS which could further enhance the growth inhibition of cancer cells. Thus ZnO nanoparticles could play an important role in the PDT. Instead of dangerous ultraviolet (UV) radiation light, NIR is a very good choice for PDT, which not only can afford deeper penetration depths, but also impose lower phototoxicity on normal cells and tissues. ZnO NPs are also known as one of photothermal (PTT) agents for cancer treatment [16, 17]. Zinc oxide nanoparticles with their ability to produce ROS, if modified to absorb NIR light instead of UV, it could be used for a dual PDT and PTT therapy and thus enhance its inherent toxicity and selectivity towards cancer cells.

Doping is mainly developed, with the aim of shifting light absorption towards higher wavelength region and simultaneous doping (co-doping) of two or three transition metals or metal ions could successfully modify the electronic structures of ZnO and shift its absorption edge to a lower energy [18]. In this study we have prepared (Ag,Cu,Co) co-doped ZnO nanostructures from thermal decomposition of novel precursors (Ag,Cu, Co) co-doped zinc laurate hydrazinate which were prepared by coprecipitation method [19]. Dopants are so choosen that they are biologically active and can tune electronic and optical property [6, 20, 21, 22]. The carboxylic acid is lauric acid which is a medium-length long-chain fatty acid having anti microbial properties [23]. Thermal decomposition of solid solution precursor metal carboxylate hydrazinate [24] has been used to prepare fine-particle mixed metal ferrites [25] cobaltites [26] and yttria [27]. These precursors once ignited, decompose in the presence of air auto catalytically, with the evolution of N_2, H_2 and CO_2 to yield fine particle oxides. Hydrazine by virtue of its coordinating ability with transition metal can act as a neutral, monodentate, bidentate and bridged bidentate ligand with metal carboxylates. The heat required for the formation of nanosized particles is provided by the combustion of hydrazine and carbonaceous mass of the carboxylate precursor. The synthesis is inexpensive, simple, fast, and yields high purity products in a single step. In this paper the preparation, characterization, optical properties of (Ag, Cu,Co) co-doped zinc oxide nanocomposites as well as the cytotoxic response in human breast cancer (MCF-7) cells and the human embryonic kidney normal cells (HEK 293) are investigated.

2. Experimental

2.1. Preparation of the precursor (Ag,Cu,Co) co-doped zinc laurate hydrazinate

The precursor was prepared by coprecipitation method. First the ethonolic solution (50ml) of lauric acid (1.020g, $0.51\mathbf{x}10^{-2}$mol) was stirred with hydrazine hydrate $N_2H_4{\_}H_2O$ (99–100%) (4 ml, 8 $\mathbf{x}10^{-2}$mol). To this, a freshly prepared aqueous solution (50 ml) of zinc nitrate hexahydrate (1.23 g, $0.4\mathbf{x}10^{-2}$mol) mixed with silver nitrate (0.1g, $0.05\mathbf{x}10^{-2}$mol), copper nitrate hexahydrate (0.05g, $0.01\mathbf{x}10^{-2}$mol) and cobalt nitrate hexahydrate (0.1g, $0.05\mathbf{x}10^{-2}$mol) was added dropwise with constant stirring. The precursor formed immediately, was kept aside for an hour for digestion, filtered, washed with water and alcohol followed by diethylether and air-dried. All reagents used for the reaction are of analytical grade.

$$\underset{\text{Metal nitrate}}{Zn(NO_3)_{2(aq)} + AgNO_3 + Cu(NO_3)_{2(aq)} + Co(NO_3)_{2(aq)}} + \underset{\text{Lauric acid}}{CH_3(CH_2)_{10}COOH} + \underset{\text{Hydrazine hydrate}}{2N_2H_4 \cdot H_2O} \rightarrow \underset{\text{(Ag,Cu,Co) co-doped zinc laurate hydrazinate}}{(Ag,Cu,Co)Zn(CH_3(CH_2)_{10}COO)(N_2H_4)_2} + 7NO_3^- + nH_2O + H^+$$

2.2. Preparation of AgCuCoZnO nanocomposites

Thermal decomposition of the precursor led to the formation of oxide nanoparticles. The dried precursor was transferred to silica crucible and heated to red hot condition in an ordinary atmosphere. The precursor got ignited, underwent autocatalytic decomposition using atmospheric oxygen resulting in the formation of fine oxide products. The obtained nanoparticles were further heated at 400˚ C to remove any residual carbon formed during the decomposition.

$$\underset{\text{(Ag,Cu,Co) co-doped zinc laurate hydrazinate}}{(Ag,Cu,Co)Zn(CH_3(CH_2)_{10}COO)(N_2H_4)_2} \xrightarrow{\Delta} \underset{\text{(Ag,Cu,Co) co-doped zinc oxide (nanocomposites)}}{AgCuCoZnO}$$

(Ag,Cu,Co) co-doped ZnO nanocomposites prepared, hereafter referred to as AgCuCoZnO nanocomposites.

2.3. Quantitative methods

The hydrazine content in the precursor was chemically determined volumetrically using 0.025 M KIO_3 as titrant under Andrew's condition [28]. Elemental analysis of C, H and N were performed on a Elementar Vario EL III analyzer. Actual doping concentration was quantified with inductively coupled plasma atomic emission spectroscopy (ICP-AES) using Thermo Electron IRIS INTREPID II XSP DUO Flexible axial and radial view instrument, with high concentration capabilities, after digesting the precursor in HNO_3, made to 50ml, filtered and analysed.

2.4. Sample characterization

All reagents for the synthesis were obtained commercially and used as received. The infrared spectrum of the solid precursor sample was recorded using KBr pellets in the range of 4000–400 cm^{-1} on Thermo Nicolet, Avatar 370-FT-IR spectrometer. EDX energy-dispersive X-ray spectroscopy was performed by SIGMA HV – Carl Zeiss with Bruker Quantax 200 – Z10 EDS Detector. The simultaneous TG-DTA experiment was carried out in Perkin Elmer, Diamond TG/DTA thermal analyzers. Thermal analysis was carried out in nitrogen atmosphere at the heating rate of 10˚ C per minute using 4.365mg of the sample. Platinum cups were used as sample holders and alumina as reference. The temperature range was ambient to 700˚ C. XRD pattern was recorded using Bruker AXS D8 Advance X-ray diffractometer using CuK_ radiation (1.5406 A°) at 40 kV and 40 mA. Scanning electron microscopy (SEM) was performed with a JEOL Model JSM - 6390LVmicroscope. The morphology of the synthesized NPs was characterized using transmission electron microscopy (TEM) Jeol/JEM 2100 model operating with an accelerating voltage of 200 kV. UV-Vis-NIR absorption spectra was recorded at room temperature on Perkin Elmer lambda 950 UV-VIS-NIR instrument with spectral range of 175–3300 nm having Deuterium lamp (UV region)and Tungsten- Halogen lamp (VIS-NIR region)as source, PMT (UV-VIS) and Peltier cooled PbS (NIR) as Detectors.

2.5. In vitro cytotoxicity

2.5.1. Cell lines and cell culture

The human breast adenocarcinoma cell line (MCF7) was obtained from National Centre for Cell Science (NCCS), Pune and grown in Eagles Minimum Essential Medium containing 10% fetal bovine serum (FBS). The cells were maintained at 370˙ C, 5% CO_2, 95% air and 100% relative humidity. Maintenance cultures were passaged weekly, and the culture medium was changed twice a week. The human embryonic kidney cell line (HEK 293) was obtained from National Centre for Cell Science (NCCS), Pune and grown in Eagles Minimum Essential Medium containing 10% fetal bovine serum (FBS). The cells were maintained at 370˙ C 5% CO2, 95% air and 100% relative humidity. Maintenance cultures were passaged weekly, and the culture medium was changed twice a week.

2.5.2. Estimation of cytotoxicity: cell treatment procedure

The monolayer cells were detached with trypsin-ethylenediaminetetraacetic acid (EDTA) to make single cell suspensions and viable cells were counted using a hemocytometer and diluted with medium containing 5% FBS to give final density of 1 × 105 cells/ml. One hundred microlitres per well of cell suspension were seeded into 96-well plates at plating density of 10,000 cells/well and incubated to allow for cell attachment at 370˙ C, 5% CO2, 95% air and 100% relative humidity. After 24h the cells were treated with serial concentrations of the test samples. They were initially dispersed by sonication in phosphate buffered saline (PBS) and an aliquot of the sample solution was diluted to twice the desired final maximum test concentration with serum free medium. Additional four serial dilutions were made to provide a total of five sample concentrations. Aliquots of 100 µl of these different sample dilutions were added to the appropriate wells already containing 100 µl of medium, resulting in the required final sample concentrations. Following sample addition, the plates were incubated for an additional 48 h at 370˙ C, 5% CO2, 95% air and 100% relative humidity. The medium without samples were served as control and triplicate was maintained for all concentrations.

2.5.3. MTT assay

[4,5-dimethylthiazol-2-yl]2,5-diphenyltetrazolium bromide (MTT)] is a yellow water soluble tetrazolium salt. A mitochondrial enzyme in living cells, succinate-dehydrogenase, cleaves the tetrazolium ring, converting the MTT to an insoluble purple formazan. Therefore, the amount of formazan produced is directly proportional to the number of viable cells. After 48 h of incubation, 15µl of MTT (5 mg/ml) in phosphate buffered saline (PBS) was added to each well and incubated at 370˙C for 4h. The medium with MTT was then flicked off and the formed formazan crystals were solubilized in 100µl of DMSO and then measured the absorbance at 570 nm using micro plate reader. The % cell inhibition was determined using the following formula, % Cell Inhibition = 100-{Abs (sample)/Abs (control) x100}.Nonlinear regression graph was plotted between % Cell inhibition and Log concentration and IC50 was determined using Graph Pad Prism software.

3. Results and discussion

3.1. Characterization of the precursor

3.1.1. Chemical analysis

The percentage of hydrazine, carbon, nitrogen, hydrogen and metals present in the precursors were analysed and given in Table 1.

3.1.2. Thermal analysis

As can be observed from Fig. 1, the precursor loses weight in two steps. From TG curve the first step is the loss of surface water molecule at a temperature range between100˙ C and 110˙ C. The corresponding peak in DTA curve is observed as an endotherm at 108˙ C. The major weight loss of 68% on the TG curve from 320˙ C to 420˙ C is attributed to the second step involving simultaneous dehydrazination and decarboxylation of the precursor. This is indicated by a sharp endothermic peak in DTA curve at 413˙ C which gives AgCuCoZnO as the final residue, which is stable over 700˙ C without any further weight loss. The thermal analysis data are given in Table 2.

Table 1
Chemical analysis of precursor.

Analysis		AgCuCo co-doped Zinc laurate Hydrazinate	
		obs	cal
Hydrazine %		16.88	17.57
Elemental Analysis %	C	37.75	37.16
	H	9.00	8.80
	N	14.68	15.89
Metal %	Zn	20.87	21.70
	Ag	2.80	2.55
	Cu	0.83	0.74
	Co	1.54	1.34

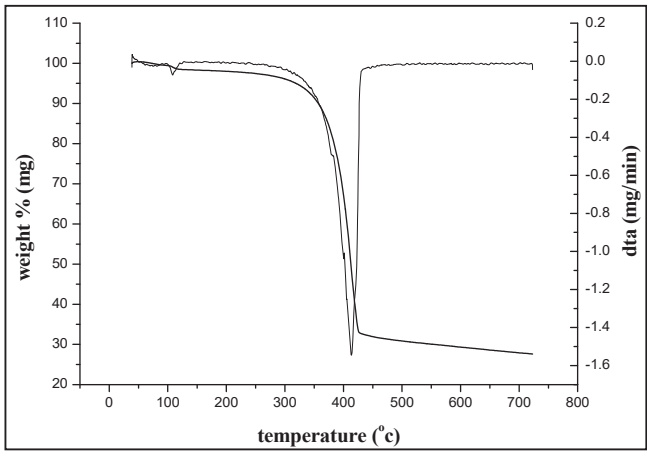

Fig. 1. Thermogravimetric-differential thermal analysis (TG-DTA) curve of precursor.

The analytical data of the precursor obtained from chemical (Table 1) and thermal (Table 2) analysis are found to be in good agreement with the values calculated, considering the molecular stoichiometric composition as $Ag_{0\cdot1}Cu_{0\cdot05}Co_{0\cdot1}Zn(C_{12}H_{23}O_2)(N_2H_4)_2$ for precursor (Ag,Cu,Co) codoped Zinc laurate hydrazinate**.**

3.1.3. FT-IR analysis

The FT-IR spectra of the precursor shown in Fig. 2 have three bands in the region (3248–3356) cm^{-1}, which are characteristic of N–H stretching frequencies. The N–N stretching frequency is observed at 972 cm^{-1}which confirms the presence of hydrazine as bidentate bridging ligand [29]. The asymmetric stretching frequencies of the carboxylate group in the precursor are observed at 1604 cm^{-1} and 1543cm^{-1}. The symmetric stretching frequencies of the carboxylate group in the precursor are observed at 1442 cm^{-1} and 1404 cm^{-1}. The (asym–sym) separation of 162 cm^{-1} and 139 cm^{-1} indicate the bidentate bridging nature of carboxylate group. These results support the formation of (AgCuCo) codoped Zn(lau)$(N_2H_4)_2$ precursor. The infrared spectra analysis data are given in Table3.

3.2. Characterization of the synthesized AgCuCoZnO nanocomposites

3.2.1. FT-IR analysis

From the FT-IR spectra in Fig. 3, we observe peak only at 490cm^{-1} for AgCuCoZnO nanocomposites, which corresponds to the metal-oxygen (Zn–O) stretching vibration. Peaks corresponding to organic species and hydrazine are completely removed. This confirms that after thermal decomposition only the metal oxide exist.

3.2.2. Energy dispersive X-ray analysis (EDX)

The EDX analysis shown in Fig. 4 exhibit the presence of metals in AgCuCoZnO nanocomposites and it is clear that there is incorporation of

Table 2
Thermal analysis of precursor.

Precursor	TG temp range °c	Mass loss %	DTA Peak temp °c	Decomposition product
(AgCuCo)co-doped Zinc laurate hydrazinate	100–110	2.31%	108 (-)	Loss of one water molecule
	320–420	68.0%	413 (-)	Loss of two N_2H_4 molecule & decarboxylation

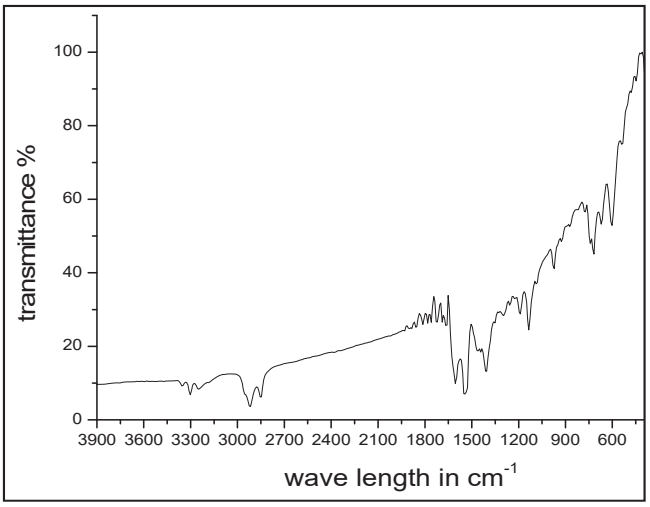

Fig. 2. FT-IR analysis of precursor.

Table 3
FT-IR analysis of precursor.

Precursor	$\nu_{O\text{-}H}$ cm^{-1}	$\nu_{N\text{-}H}$ cm^{-1}	$\nu_{asy\ o=c=o}$ cm^{-1}	$\nu_{sy\ o=c=o}$ cm^{-1}	$\Delta\nu$ cm^{-1}	$\nu_{N\text{-}N}$ cm^{-1}
(Ag,Cu,Co)co-doped Zinc laurate hydrazinate	—	3248–3356	1604 1543	1442 1404	162 139	972

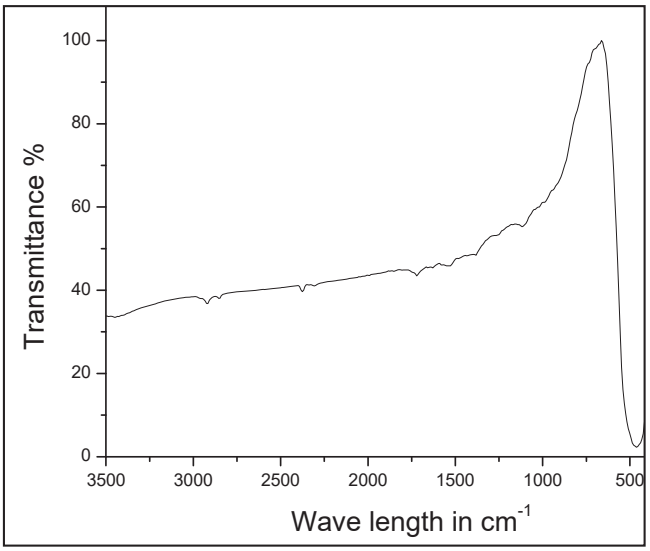

Fig. 3. FT-IR spectra of AgCuCoZnO nanocomposites.

all metal dopants and no other elemental impurities present in the synthesized nanostructures.

3.2.3. ICP-AES analysis

The compositions of nanocomposites were analysed using ICP-AES and given in Table 4. The estimated values of metals agreed with the expected values. This result confirms the absence of loss of elements during thermal decomposition.

3.2.4. X-ray diffraction pattern (XRD)

A typical XRD pattern of AgCuCoZnO nanocomposites is shown in Fig. 5, which shows planes corresponding to both wurtzite phase of ZnO and face-centered cubic (fcc) phase of metallic Ag. The peaks at 31.70°, 34.39°, 36.19°,47.51°, 56.55°, 62.86°, 67.93°, 69.03° can respectively be indexed to (100), (002), (101), (102), (110), (103), (112) and (201) planes of hexagonal wurtzite ZnO structure (JCPDS No36-1451). The three diffraction peaks observed at 38.05°, 44.22° and 77.49° correspond respectively to (111), (200) and (311) planes of the face-centered cubic structure of Ag (JCPDS No 04–0783). The results suggest that silver is not getting incorporated into the zinc oxide lattice but rather forms on the surface of zinc oxide as metallic silver [30]. No obvious intensity peak of metallic Co, Cu or related compounds is detected under the sensitivity of an X-ray diffractometer, which rules out the possibility of any secondary phase. Thus the dopants (Co and Cu) are well doped in the ZnO lattice. The average particle size is calculated using Debye-Scherrer formula, $D = K\lambda/\beta \cos\theta$, where D is crystallite size (nm), θ is Bragg diffraction angle, λ is the source wavelength (1.54) and β is the width of the XRD peak at half maximum height. The calculated average particle size of AgCuCoZnO nanocomposites is found to be around 16nm.

3.2.5. SEM and TEM analysis

The SEM image shows the external morphology of nanoparticles. From Fig. 6 AgCuCoZnO nanocomposites exhibit that, the majority of particles are of polygonal shape. From TEM micrographs in Fig. 7 the average diameter is calculated, from measuring over 100 particles in random fields of TEM view. The average TEM diameter of AgCuCoZnO nanocomposites is between 10 to 20 nm, supporting the XRD data. The selected area electron diffraction (SAED) pattern of AgCuCoZnO nanocomposites have sharp spots indicative of polycrystalline nature with symmetrical orientation as shown in Fig. 8.

3.2.6. UV-VISIBLE-NIR absorption spectra

ZnO NPs respond only to UV light. Absorption spectra for AgCuCoZnO nanocomposites present a significant absorbance in the visible and NIR region as shown in Fig. 9. X-Ray diffraction reveals the presence of metallic Ag on the surface of ZnO lattice. The Metal dopants (Co and Cu) can narrow the band gap of ZnO NPs by introducing new energy levels between VB and CB and reduce the carrier recombination centers, thereby achieving the enhancement of visible-light absorption. Metallic Ag which has strong electron accepting ability suggest strong interfacial electronic coupling between Ag and CuCoZnO and shows surface plasmon resonance. The surface plasmon absorption maximum red shifts to the NIR region when Ag nanoparticles form assemblies or aggregates [31].

3.2.7. In vitro cytotoxicity AgCuCoZnO nanocomposites

The synthesized AgCuCoZnO nanocomposites were tested for their potent cytotoxic activity against human breast cancer cells (MCF-7) and human embryonic kidney normal cell line (HEK 293) using MTT assay. MCF-7 and HEK 293 cell viability were evaluated after 48 h exposure to AgCuCoZnO nanocomposites of various concentrations ranging from (6.25 μg/ml to 50 μg/ml). The living cells, convert the MTT assay to an insoluble purple formazan. The quantity of formazan (presumably directly proportional to the number of viable cells) is measured by recording changes in absorbance at 570 nm using micro plate reader. The % cell viability of the nanocomposites towards cancer and normal cell lines were determined using the following formula, % Cell viability = {Abs (sample)/Abs (control) x100} and shown in Fig. 10.

3.2.7.1. Evaluation of IC50 value. Fig. 11 shows the Nonlinear regression graph plotted between % Cell inhibition and Log concentration. IC50 was determined using Graph Pad Prism software**.** Here we present novel findings that cancerous cells are markedly more susceptible (1.8 times) to AgCuCoZnO nanocomposites mediated toxicity than their normal counterparts (the IC50 value 22 μg/ml for cancer cells and 40 μg/ml for normal cells). At lower concentrations AgCuCoZnO nanocomposite are

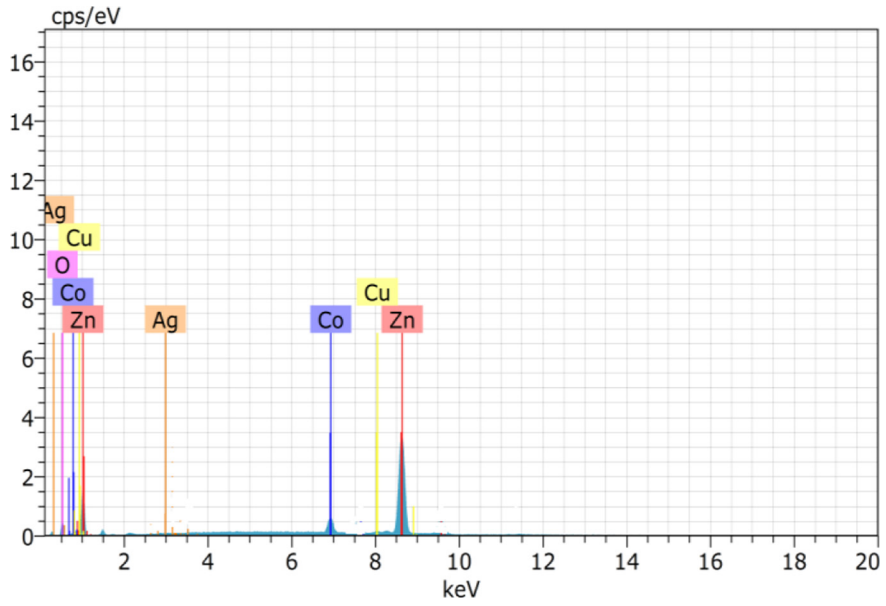

Fig. 4. EDS of AgCuCoZnO nanocomposites.

Table 4
Composition of AgCuCoZnO nanocomposites obtained from ICP-AES analysis.

Nanocomposite	Zn%		Ag%		Cu%		Co%	
	Obs	Cal	Obs	Cal	Obs	Cal	Obs	Cal
AgCuCoZnO	60.01	60.62	7.44	8.14	2.11	2.41	4.00	4.48

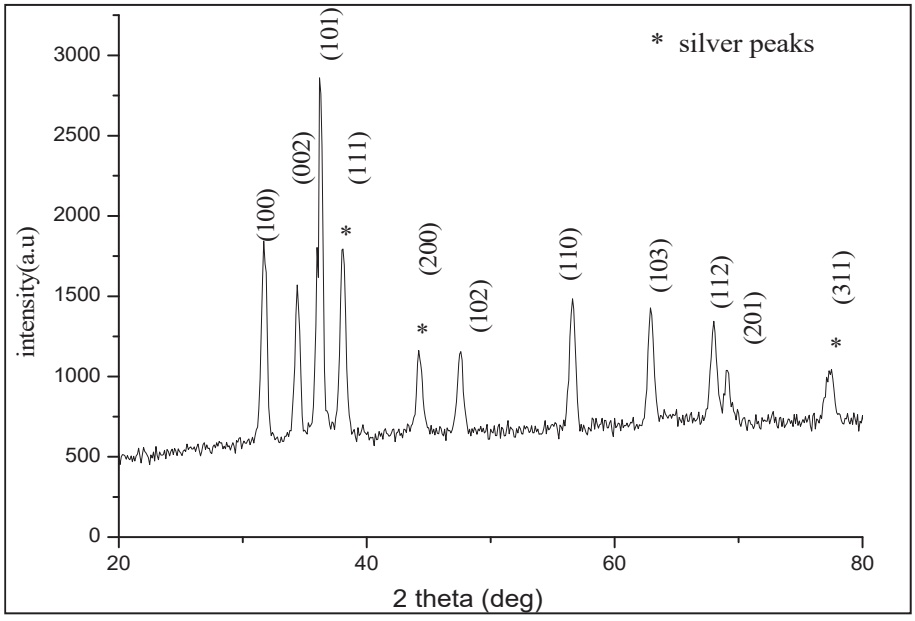

Fig. 5. X-ray diffraction pattern of AgCuCoZnO nanocomposites.

less toxic to normal cells. It is necessary to reduce IC50 to nanomolar concentrations, so that it is non toxic to normal cells. The interesting fact at this juncture is AgCuCoZnO nanocomposites absorb in near-infrared (NIR) region. NIR absorption is critical for both photo dynamic therapy and photo thermal therapy because of minimal light absorption by water and hemoglobin and the resulting optimal tissue penetration of the light in this region. AgCuCoZnO nanocomposites on irradiating with NIR light may produce greater level of ROS and can heat up the cancer tissues. The inherent toxicity of AgCuCoZnO nanocomposites along with combined therapy of PDT and PTT may reduce the IC50 to nanomolar concentrations and further improve the cancer cell toxicity. Thus these AgCuCoZnO nanocomposites can act as a potential candidate for developing anti-cancer therapeutics. ROS generation is proposed as one of the key cytotoxic mechanism [7, 8] for ZnO nanoparticles. The mechanism of cytotoxicity of AgCuCoZnO nanocomposites is not fully understood.

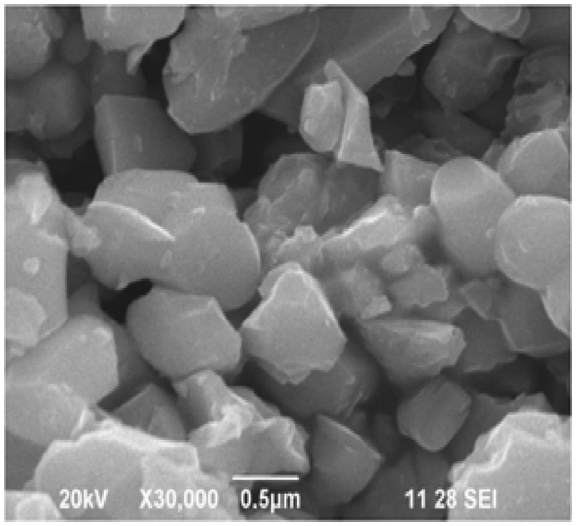

Fig. 6. SEM image of AgCuCoZnO nanocomposites.

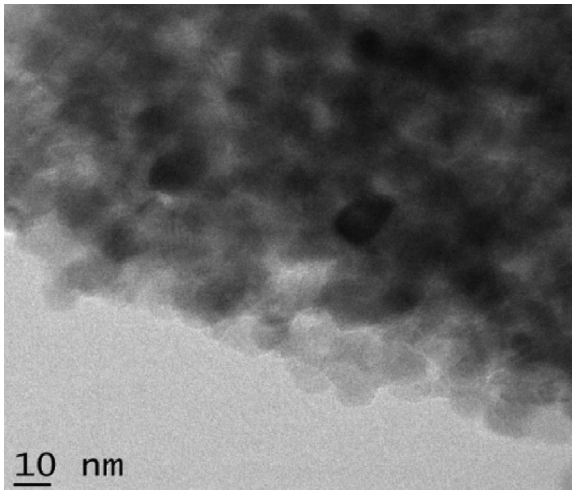

Fig. 7. TEM image of AgCuCoZnO nanocomposites.

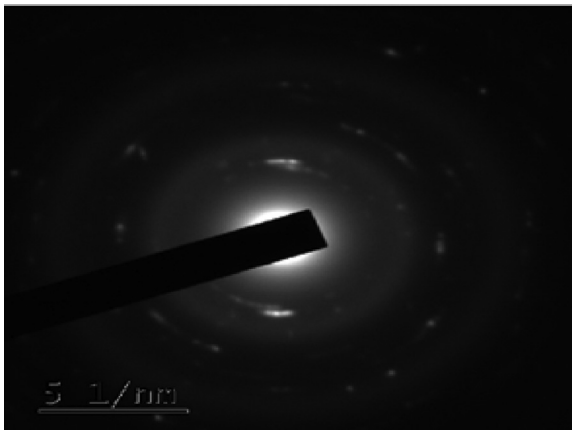

Fig. 8. SAED pattern of AgCuCoZnO nanocomposites.

4. Conclusion

The synthesis of AgCuCoZnO nanocomposites were successfully achieved by a simple thermal decomposition method. Primarily, the composition, morphology and optical properties were determined. The cytotoxicity of the AgCuCoZnO nanostructures against human breast cancer cells (MCF-7) and the human embryonic kidney normal cells (HEK 293) in vitro were studied. We present the finding that cancerous cells are markedly more susceptible than normal cells. As the nanocomposites have strong absorption in the visible and NIR region, they can be used as photosensitizers for PDT/PTT. The selective cytotoxicity of the nanocomposites against cancer cells can be improved by irradiating with visible or NIR light. Thus these novel nanocomposites are promising material for cancer therapy. Further research on anticancer activity of AgCuCoZnO nanocomposites in different types of cancer cells is warranted. A great amount of work is still needed to develop practical applications of these novel nanomaterials.

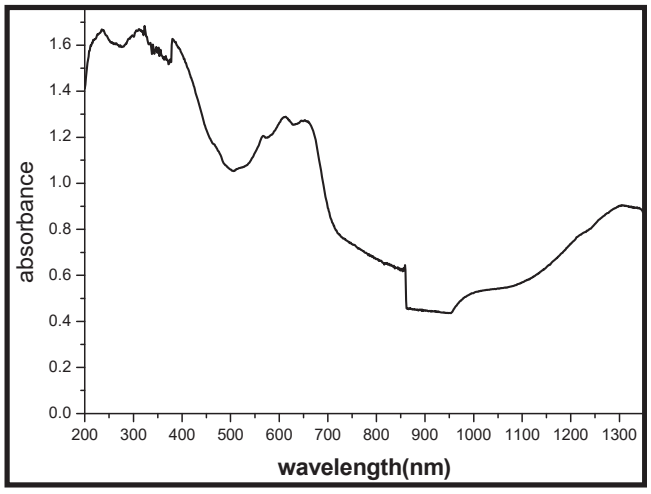

Fig. 9. UV-VISIBLE-NIR absorption spectra of AgCuCoZnO nanocomposites.

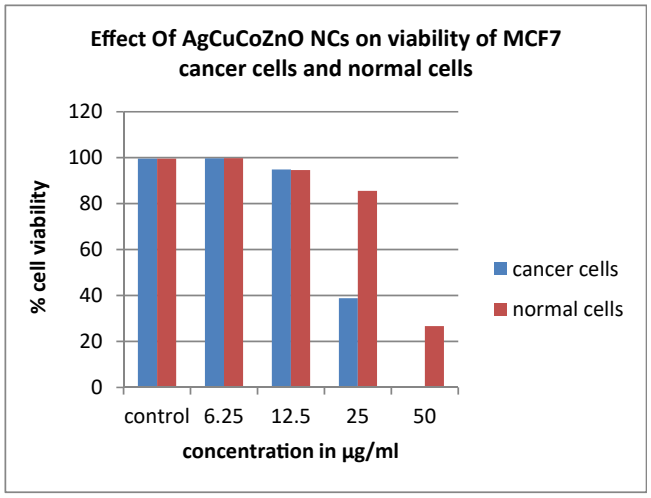

Fig. 10. The percentage viability of MCF7 cancer cell lines and HEK 293 normal cell lines using MTT assay after 48 h exposure to AgCuCoZnO (6.25–50 μg/mL). Data represented are mean ± standard deviation of three identical experiments made in triplicate.

Declarations

Author contribution statement

K Vasuki, R Manimekalai: Conceived and designed the experiments; Contributed reagents, materials, analysis tools or data; Performed the experiments; Analyzed and interpreted the data; Wrote the paper.

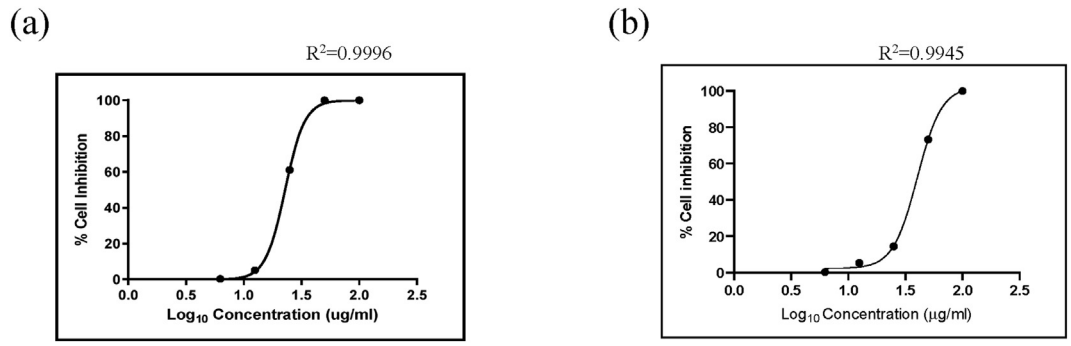

Fig. 11. Cytotoxicity of AgCuCoZnO against (a) cancer cell line (MCF 7) IC50 value 22 µg/ml and (b) normal kidney (HEK 293) cell line IC 50 value 40 µg/ml.

Funding statement

This research did not receive any specific grant from funding agencies in the public, commercial, or not-for-profit sectors.

Competing interest statement

The authors declare no conflict of interest.

Additional information

No additional information is available for this paper.

Acknowledgements

The authors are thankful to Kongunadu Arts and Science College, Coimbatore, for providing facilities. We acknowledge the provision of necessary facilities by SAIF Cochin, IIT Madras, Karunya University, Coimbatore and KMCH College of Pharmacy Coimbatore.

References

[1] J. Fang, H. Nakamura, H. Maeda, The EPR effect: unique features of tumor blood vessels for drug delivery, factors involved, and limitations and augmentation of the effect, Adv. Drug Deliv. Rev. 63 (2011) 136–151.
[2] R. Augustine, A.P. Mathew, A. Sosnik, Metal oxide nanoparticles as versatile therapeutic agents modulating cell signaling pathways: linking nanotechnology with molecular medicine, Appl. Mater. Today 7 (2017) 91–103.
[3] L.R. Yang, M. Yu, F. Bai, C. Li, Z.L. Wang, Cellular level biocompatibility and biosafety of ZnO nanowires, J. Phys. Chem. C 112 (2008) 20114–20117.
[4] N. Jones, B. Ray, K.T. Ranjit, A.C. Manna, Antibacterial activity of ZnO nanoparticle suspensions on a broad spectrum of microorganisms, FEMS (Fed. Eur. Microbiol. Soc.) Microbiol. Lett. 279 (2008) 71–76.
[5] M. Premanathan, K. Karthikeyan, K. Jeyasubramanian, G. Manivannan, Selective toxicity of ZnO nanoparticles toward gram-positive bacteria and cancer cells by apoptosis through lipid peroxidation, Nanomed. Nanotechnol. Biol. Med. 7 (2011) 184–192.
[6] P. Sivakumar, M. Lee, Y.S. Kim, M.S. Shim, Photo-triggered antibacterial and anticancer activities of zinc oxide nanoparticles, J. Mat. Chem. B 6 (2018) 4852–4871.
[7] C.T. Ng, L.Q. Yong, M.P. Hande, C.N. Ong, L.E. Yu, B.H. Bay, G.H. Baeg, Zinc oxide nanoparticles exhibit cytotoxicity and genotoxicity through oxidative stress responses in human lung fibroblasts and Drosophila melanogaster, Int. J. Nanomed. 12 (2017) 1621–1637.
[8] J.W. Rasmussen, E. Martinez, P. Louka, D.G. Wingett, Zinc oxide nanoparticles for selective destruction of tumor cells and potential for drug delivery applications, Expert Opin. Drug Deliv. 7 (2010) 1063–1077.
[9] C. Hanley, J. Layne, A. Punnoose, K.M. Reddy, I. Coombs, A. Coombs, K. eris, D. Wingett, Preferential killing of cancer cells and activated human T cells using ZnO nanoparticles, Nanotechnology 19 (2008), 295103.
[10] U. Chitgupi, Y. Qin, J.F. Lovell, Targeted nanomaterials for phototherapy, Nanotheranostics 1 (2017) 38–58.
[11] M. Triesscheijn, P. Baas, J.H.M. Schellens, F.A. Stewart, Photodynamic therapy in oncology, The Oncologist 11 (2006) 1034–1044.
[12] J. Van der Zee, Z. Vujaskovic, M. Kondo, T. Sugahara, The Kadota fund international forum 2004–clinical group consensus*, Int. J. Hyperth. 24 (2008) 111–122.
[13] X. Huang, G. Chen, J. Pan, X. Chen, N. Huang, X. Wang, J. Liu, Effective PDT/PTT dual-modal phototherapeutic killing of pathogenic bacteria by using ruthenium nanoparticles, J. Mater. Chem. B 4 (2016) 6258–6270.
[14] J. Oh, H. Yoon, J.H. Park, Nanoparticle platforms for combined photothermal and photodynamic therapy, Biomed. Eng. Lett. 3 (2013) 67–73.
[15] Z. Chen, Q. Wang, H. Wang, L. Zhang, G. Song, L. Song, J. Hu, H. Wang, J. Liu, M. Zhu, D. Zhao, Ultrathin PEGylated $W_{18}O_{49}$ Nanowires as a new 980 nm-laser-driven photothermal agent for efficient ablation of cancer cells in vivo, Adv. Mater. 25 (2013) 2095–2100.
[16] K. Vimala, K. Shanthi, S. Sundarraj, S. Kannan, Synergistic effect of chemo-photothermal for breast cancer therapy using folic acid (FA) modified zinc oxide nanosheet, J. Colloid Interface Sci. 488 (2017) 92–108.
[17] S. Kim, S.Y. Lee, H.J. Cho, Berberine and zinc oxide-based nanoparticles for the chemo-photothermal therapy of lung adenocarcinoma, Biochem. Biophys. Res. Commun. 501 (2018) 765–770.
[18] F.-R. Wang, Y.-Y. Su, J.-K. Liu, Y. Wub, Enhanced photoelectric properties by the coordinating role of doping and modification, Phys. Chem. Chem. Phys. 18 (2016) 4850–4859.
[19] L. Vikram, B.N. Sivasankar, Spectral, thermal and X-ray studies on some new bis-hydrazine metal glyoxylates and bis-hydrazine mixed metal glyoxylates, Thermochim. Acta 452 (2007) 20–27.
[20] J. Gupta, J. Mohapatra, D. Bahadur, Visible light driven mesoporous Ag-embedded ZnO nanocomposite:reactive oxygen.species enhanced photocatalysis, bacterial inhibition and photodynamic therapy, Dalton Trans. 46 (2017) 685–696.
[21] S. Kuriakose, B. Satpati, S. Mohapatra, Enhanced photocatalytic activity of Co doped ZnO nanodisks and nanorods prepared by a facile wet chemical method, Phys. Chem. Chem. Phys. 16 (2014) 12741.
[22] S.A. Khan, F. Noreen, S. Kanwal, A. Iqbal, G. Hussain, Green synthesis of ZnO and Cu-doped ZnO nanoparticles from leaf extracts of Abutilon indicum, Clerodendrum infortunatum , Clerodendrum inerme and investigation of their biological and photocatalytic activities, Mater. Sci. Eng. C 82 (2018) 46–59.
[23] T. Nakatsuji, M.C. Kao, J.Y. Fang, C.C. Zouboulis, L. Zhang, R.L. Gallo, C.M. Huang, Antimicrobial property of lauric acid against propionibacterium acnes: its therapeutic potential for inflammatory acne vulgaris, J. Investig. Dermatol. 129 (2009) 2480–2488.
[24] K. C Patil, M.S. Hegde, T. Rattan, S.T. Aruna, Combustible solid precursors to nanocrystalline oxide materials, Chem. Nanocryst. Oxide Mater. (2008) 9–41.
[25] P. Ravindranathan, K.C. Patil, Novel solid solution precursor method for the preparation of ultrafine Ni-Zn ferrites, J. Mater. Sci. 22 (1987) 3261.
[26] R. Selvakumar, S.J. Geib, T. Premkumar, S. Vairam, S. Govindarajan, Isomorphic metal malonates with N-aminoguanidine: MCo_2O_4 (M = Ni & Zn) nanoparticle synthesis via a $(AmgH)_2[M_{1/3}Co_{2/3}(mal)_2(H_2O)_2]$ precursor solid solution, New J. Chem. (40) (2016) 257–264.
[27] S. Ekambaram, K.C. Patil, Combustion synthesis of yttria, J. Mater. Chem. 5 (1995) 905–908.
[28] W. Schmidt, The reactions of hydrazine with transition-metal complexes, in: Hydrazine and its Derivatives, Wiley, New York, 1985.
[29] A. Braibanti, F. Dallevalle, M.A. Pellinghelli, E. Leopardi, The nitrogen-nitrogen stretching band in hydrazine derivatives and complexes, Inorg. Chem. 7 (1968) 1430–1433.
[30] R.J.V. Michael, B. Sambandam, T. Muthukumar, M.J. Umapathy, P.T. Manoharan, Spectroscopic dimensions of silver nanoparticles and clusters in ZnO matrix and their role in bioinspired antifouling and photocatalysis, Phys. Chem. Chem. Phys. 16 (2014) 8541.
[31] Y. Liang, N. Guo, L. Li, R. Li, G. Ji, S. Gan, Facile synthesis of Ag/ZnO micro-flowers and their improved ultraviolet and visible light photocatalytic activity, New J. Chem. 40 (2016) 1587–1594.